

Random Primordial Magnetic Fields and the Gas Content of Dark Matter Haloes

Rafael S. de Souza^{1*}, Luiz Felipe S. Rodrigues^{1†}, and Reuven Opher^{1‡}

¹*IAG, Universidade de São Paulo, Rua do Matão 1226, Cidade Universitária, CEP 05508-900, São Paulo, SP, Brazil*

Accepted – Received –

ABSTRACT

We recently predicted the existence of random primordial magnetic fields (RPMF) in the form of randomly oriented cells with dipole-like structure with a cell size L_0 and an average magnetic field B_0 . Here we investigate models for primordial magnetic field with a similar web-like structure, and other geometries, differing perhaps in L_0 and B_0 . The effect of RPMF on the formation of the first galaxies is investigated. The filtering mass, M_F , is the halo mass below which baryon accretion is severely depressed. We show that these RPMF could influence the formation of galaxies by altering the filtering mass and the baryon gas fraction of a halo, f_g . The effect is particularly strong in small galaxies. We find, for example, for a comoving $B_0 = 0.1 \mu\text{G}$, and a reionization epoch that starts at $z_s = 11$ and ends at $z_e = 8$, for $L_0 = 100 \text{ pc}$ at $z = 12$, the f_g becomes severely depressed for $M < 10^7 M_\odot$, whereas for $B_0 = 0$ the f_g becomes severely depressed only for much smaller masses, $M < 10^5 M_\odot$. We suggest that the observation of M_F and f_g at high redshifts can give information on the intensity and structure of primordial magnetic fields.

Key words: galaxies: formation, haloes – magnetic fields – large scale structure of Universe

1 INTRODUCTION

Understanding the details of galaxy formation remains an important challenge in cosmology. As shown by numerical calculations, the first generation of galaxies should have formed at very high redshifts inside collapsing halos, starting at $z \sim 65$, corresponding to high peaks of the primordial dark matter (DM) density field (Naoz et al. 2006). Cosmic Microwave Background (CMB) radiation observations suggest that reionization began at high redshifts. This means that a high abundance of luminous objects must have existed at that time, since these first luminous objects are expected to have heated and reionized their surroundings (Barkana & Loeb 2001; Wyithe & Loeb 2003; Haiman & Holder 2003; Cen 2003).

The formation of a luminous object inside a halo necessarily requires the existence of baryonic gas there. Even in halos that are too small for cooling via atomic hydrogen, the gas content can have substantial, and observable, astrophysical effects. In addition to the possibility of hosting astrophysical sources, such as stars, small halos may pro-

duce a 21-cm signature (Kuhlen et al. 2006; Shapiro et al. 2006; Naoz & Barkana 2008; Furlanetto & Oh 2006), and can block ionizing radiation and produce an overall delay in the global progress of reionization (Barkana & Loeb 2002; Iliiev et al. 2003, 2005; McQuinn et al. 2007).

The evolution of the halo gas fraction at various epochs of the Universe is of prime importance, particularly in the early Universe. We evaluate here the possible influence of a primordial magnetic field on the halo gas fraction.

As noted by Gnedin (2000); Gnedin & Hui (1998), both in the linear and non-linear regimes, the accretion of gas into DM halos is suppressed below a characteristic mass scale called the filtering mass, M_F . This mass scale coincides with the Jeans mass, M_J , if the latter does not vary in time. Otherwise, M_F is a time average of M_J . Thus, an increase in the ambient pressure in the past, causes an increase in M_J and suppresses the accretion of baryons into DM halos in a cumulative fashion, producing an increase in M_F .

Until now, studies focused on the UV heating of the neutral interstellar gas as the main source of pressure, for determining the filtering mass. These results are widely used in many semi-analytic models (e.g. Macciò et al. 2010), particularly those designed to study the properties of small galaxies (due to the high redshift character of the UV heating).

In this paper we add the effect of a possible random

* Email: rafael@astro.iag.usp.br

† Email: felippe@astro.iag.usp.br

‡ Email: opher@astro.iag.usp.br

primordial magnetic field as another important source of ambient pressure. The magnetic field contributes to pressure support, which changes the Jeans mass and, consequently, the filtering mass and the quantity of gas that is accreted by DM halos.

The paper is organized as follows. In section 2 we make a short review on the possible origins of primordial magnetic fields, in section 3 we analyze the effect of primordial magnetic fields on the Jeans and filtering masses and in section 4 we calculate effects on the baryon mass fraction. In section 5 we give our conclusions.

2 PRIMORDIAL MAGNETIC FIELDS

The origin of large-scale cosmic magnetic fields in galaxies and protogalaxies remains a challenging problem in astrophysics (Zweibel & Heiles 1997; Kulsrud & Zweibel 2008; de Souza & Opher 2008; de Souza & Opher 2010a,b; Widrow 2002; Laganá et al. 2010). Understanding the origin of the structures of the present Universe requires a knowledge of the origin of magnetic fields. The magnetic fields fill interstellar and intracluster space and affect the evolution of galaxies and galaxy clusters. There have been many attempts to explain the origin of cosmic magnetic fields. One of the most popular astrophysical theories for creating seed primordial fields is that they were generated by the Biermann mechanism (Biermann 1950). It has been suggested that this mechanism acts in diverse astrophysical systems, such as large scale structure formation (Peebles 1967; Rees & Reinhardt 1972; Wasserman 1978), protogalaxies (Davies & Widrow 2000), cosmological ionizing fronts (Gnedin 2000), star formation and supernova explosions (Hanayama et al. 2005; Miranda et al. 1998). Another mechanism for creating cosmic magnetic fields was suggested by Ichiki et al. (2006). They investigated the second-order couplings between photons and electrons as a possible origin of magnetic fields on cosmological scales before the epoch of recombination. Studies of magnetic field generation, based on cosmological perturbations, have also been made (Takahashi et al. 2005, 2006; Clarke et al. 2001; Maeda et al. 2009).

In our galaxy, the magnetic field is coherent over kpc scales with alternating directions in the arm and inter-arm regions (e.g., Kronberg 1994; Han 2008). Such alternations are expected for magnetic fields of primordial origin (Grasso & Rubinstein 2001).

Various observations put upper limits on the intensity of a homogeneous primordial magnetic field. Observations of the small-scale cosmic microwave background (CMB) anisotropy yield an upper comoving limit of 2.98 nG for a homogeneous primordial field (Yamazaki et al. 2010). Reionization of the Universe puts upper limits of $\sim 0.7 - 3$ nG for a homogeneous primordial field, depending on the assumptions of the stellar population that is responsible for reionizing the Universe (Schleicher et al. 2008).

de Souza & Opher (2008); de Souza & Opher (2010b) suggested that the fluctuations of the plasma predicted by the Fluctuation Dissipation Theorem, after the quark-hadron transition (QHT), is a natural source for a present primordial magnetic field. They evolved the fluctuations after the QHT to the present era and predict a present cos-

mic web of random primordial magnetic fields. The average magnetic field predicted by them over a region of size L is $B = 9 \mu\text{G} (0.1 \text{ pc}/L)^{3/2}$. An average magnetic field 0.003 nG over a 2 kpc region at $z \sim 10$ is, thus, predicted.

3 EFFECTS ON THE FILTERING MASS

3.1 The filtering scale

Following the procedure of a previous work (Rodrigues et al. 2010), which studied the effects of a homogeneous primordial magnetic field, we study here the influence of random inhomogeneous primordial magnetic fields (RPMF) on the filtering mass M_F . This quantity describes the highest DM mass scale for which the baryon accretion is suppressed significantly, as we will discuss below.

First, we define the filtering scale (Gnedin & Hui 1998) as the characteristic length scale over which the baryonic perturbations are smoothed out as compared to the dark matter ones as

$$\frac{\delta_b}{\delta_{tot}} = 1 - \frac{k^2}{k_F^2}, \quad (1)$$

where δ_b is the density contrast of baryonic matter and δ_{tot} , the total density contrast. For k comparable to k_F , the density contrast δ_b is severely depressed.

As was shown by Gnedin (2000), we can relate the comoving wavenumber associated with this length scale with the Jeans wavenumber by the equation

$$\frac{1}{k_F^2(a)} = \frac{3}{a} \int_0^a \frac{da'}{k_J^2(a')} \left[1 - \left(\frac{a'}{a} \right)^{\frac{1}{2}} \right], \quad (2)$$

where a flat matter dominated universe is assumed.

One finds that the overall suppression of the growth of baryonic density perturbations depends on a time-average of the Jeans scale. By translating the length scales into mass scales, we can then define the Jeans mass and filtering mass,

$$M_J \equiv \frac{4\pi}{3} \bar{\rho} \left(\frac{2\pi a}{k_J} \right)^3 \quad \text{and} \quad M_F \equiv \frac{4\pi}{3} \bar{\rho} \left(\frac{2\pi a}{k_F} \right)^3. \quad (3)$$

From equations (3) and (2), we can write,

$$M_F^{\frac{2}{3}} = \frac{3}{a} \int_0^a da' M_J^{\frac{2}{3}}(a') \left[1 - \left(\frac{a'}{a} \right)^{\frac{1}{2}} \right], \quad (4)$$

where $\bar{\rho}$ is the mean matter density.

The commonly used Jeans mass, with negligible magnetic fields, is the mass when the gravitational pressure at the surface of a sphere of radius R_J balances the thermal pressure. An adiabatic compression of the sphere by a change in radius δR increases the thermal pressure above the gravitational pressure, causing the sphere to increase its radius and oscillate about the equilibrium value R_J .

When the thermal pressure is negligible and we only have random magnetic fields in the sphere, the definition of the Jeans mass is similar. It is the mass when the magnetic pressure at the surface balances the gravitational pressure. An adiabatic compression of the sphere of radius R_J by a change in radius δR increases the magnetic pressure above the gravitational pressure, making the sphere, again, increase its radius and oscillate about the radius R_J .

3.2 Magnetic fields and pressure

For a random magnetic field, the magnetic pressure in a region of comoving size L greater than the comoving size of a magnetic cell, L_0 , is given by (Hindmarsh & Everett 1998)

$$P = \frac{B_{rms}^2}{8\pi}, \quad (5)$$

with the following expression for the rms average of the field (Grasso & Rubinstein 2001; de Souza & Opher 2008)

$$B_{rms}(a) = \sqrt{\langle B^2 \rangle} = B_0 \left(\frac{L_0}{L} \right)^p \left(\frac{a_0}{a} \right)^2, \quad (6)$$

where B_0 is the field intensity in an individual cell, and the parameter p depends on the geometry of the field considered (section 3.5).

For $L < L_0$, the average is being made inside a single cell. Thus, the field is indistinguishable from a homogeneous field (Rodrigues et al. 2010), and we have

$$B_{rms}(a) = B_0 \left(\frac{a_0}{a} \right)^2. \quad (7)$$

3.3 Turbulence

Equations (6) and (7) can be improved taking into account the turbulent enhancement of B at large length scales, which occurs until B reaches equipartition with the kinetic energy of the plasma. An inverse cascade effect occurs, where small magnetic structures merge to form larger magnetic structures, transferring energy to larger length scales. Numerical simulations suggest that the total enhancement can be written as $f_T(t) \simeq e^{t/\tau}$, where τ is the eddy turn over time of the intergalactic turbulence. The mean value of τ is $\tau \sim 10^9$ years (Ryu et al. 2008).

Thus, equations (6) and (7) become

$$\langle B^2 \rangle = f_T^2(z) B_0^2 \left(\frac{L_0}{L} \right)^{2p} (1+z)^4 \quad \text{for } L > L_0, \quad (8)$$

$$\langle B^2 \rangle = f_T^2(z) B_0^2 (1+z)^4 \quad \text{for } L < L_0. \quad (9)$$

When the field reaches equipartition, the turbulent amplification stops. To take into account this effect in our calculations, we set an upper limit to the magnetic field of $B \approx 0.1 \mu\text{G}$ for the comoving strength of the field when averaged over 1 kpc. This is consistent with the expected values for magnetic fields in equipartition with the environment in regions around clusters and groups (Ryu et al. 2008).

This also consistent with tests that we made stopping the amplification when $\langle B^2 \rangle \sim 8\pi \rho kT$.

3.4 Obtaining the Jeans mass

It is to be noted that it is not the Alfvénic speed, determined by B_0 , which sets the timescale for an overdensity to respond to perturbations. A simple example shows this. Let a perturbation be made along the magnetic field, B_0 , in a given cell on the surface of the sphere. In that cell the Alfvénic speed is determined by B_0 . Let us assume that the perturbation enters a neighboring cell that could have its field B_0 perpendicular to the direction of propagation of the perturbation. In this neighboring cell the Alfvénic velocity of the perturbation is zero since Alfvénic perturbations can propagate only along the field. From the above example,

we conclude that in a sphere of randomly oriented cells, the velocity of perturbations is not the Alfvén velocity defined by B_0 , but is determined by the average magnetic pressure determined by $B_{rms}^2 (\ll B_0^2)$.

We are interested in obtaining the appropriate Jeans wave number, k_J , for a sphere of radius L containing randomly oriented magnetic cells of size L_0 with average magnetic fields B_0 . The usually used k_J , when magnetic fields are negligible, is $k_J = a\sqrt{4\pi G\rho}/c_s$, where c_s is the speed of sound. In such a sphere, the speed of sound sets the timescale for an overdensity to respond to perturbations, and is directly related to the pressure.

In a sphere with a homogeneous magnetic field, B_H , the speed of a perturbation propagating perpendicular to B_H is $v_{ma} = \sqrt{\frac{B_H^2}{4\pi\rho} + c_s^2}$, the magneto-acoustic velocity, which sets the timescale. The energy density in the sphere is $\frac{B_H^2}{4\pi}$.

In our case of random magnetic fields, the average energy density in the sphere is $\frac{B_{rms}^2}{4\pi}$. We may, then, expect that the characteristic velocity in our sphere of random magnetic cells is approximately given by the expression for the magneto-acoustic velocity given above, with the energy density $\frac{B_H^2}{4\pi}$ replaced by $\frac{B_{rms}^2}{4\pi}$. Defining an effective Alfvén velocity by $\bar{v}_A^2 = \frac{B_{rms}^2}{4\pi\rho}$, the characteristic velocity of a perturbation in our sphere is, then, $v_c = \sqrt{c_s^2 + \bar{v}_A^2}$.

Replacing c_s by v_c (in the usual expression for k_J when there is negligible magnetic fields) we then have

$$\frac{k_J}{a} = \left(\frac{4\pi G\rho}{c_s^2 + \bar{v}_A^2} \right)^{1/2}, \quad (10)$$

which we use in this paper.

Thus, the Jeans mass of a plasma, subject to magnetic pressure, is given by

$$M_J^2 = \frac{3}{4\pi G^3 \bar{\rho}} \left(\frac{B_{rms}^2}{4\pi\rho} + \frac{3}{2} \frac{k_B T}{m_H \mu} \right)^3, \quad (11)$$

where we use $c_s = \sqrt{\gamma k_B T / (\mu m_H)}$, with m_H being the mass of a hydrogen atom, μ the mean molecular weight and k_B the Boltzmann constant.

This expression generalizes previous calculations of the Jeans mass which only considered its limiting cases: $B \rightarrow 0$, the usual Jeans mass (e.g. Padmanabhan 2002), or $T \rightarrow 0$, the magnetic Jeans mass (e.g. Tashiro & Sugiyama 2005).

In order to choose the correct B_{rms} from either equation (6) or (7), we first calculate the (comoving) Jeans length, L_m , from equations (7) and (11), in which we assume a multi-cell regime

$$L_m^6 = \left(\frac{\kappa}{G} \right)^3 \left[\frac{\kappa f_T^2(z) B_0^2}{3} \left(\frac{L_0}{L_m} \right)^{2p} + \frac{3}{2} \frac{k_B T(z)}{\mu m_H} (1+z)^{-1} \right]^3. \quad (12)$$

where $\kappa \equiv \frac{2G}{\Omega_{m0} H_0^2}$ and we used

$$\bar{\rho} = \Omega_{m0} \frac{3H_0^2}{8\pi G} (1+z)^3 = \frac{3}{4\pi} \frac{(1+z)^3}{\kappa},$$

and

$$L_m^3 = \frac{M_J}{\frac{4}{3}\pi\bar{\rho}} (1+z)^3 = \kappa M_J.$$

If $L_m > L_0$, then L_m is the comoving Jeans length and

the Jeans mass is given by the solution of

$$M_J^2 = \frac{\kappa}{G^3} \left[\frac{\kappa^{(1-\frac{2}{3}p)}}{3} \frac{f_T^2(z) B_0^2 L_0^{2p}}{M_J^{\frac{2}{3}p}} + \frac{3}{2} \frac{k_B T(z)}{\mu m_H (1+z)} \right]^3. \quad (13)$$

If $L_m < L_0$, then the average is done inside a single cell, using equation (7), and the Jeans mass is given by

$$M_J^2 = \frac{\kappa}{G^3} \left[\frac{\kappa}{3} f_T^2(z) B_0^2 + \frac{3}{2} \frac{k_B T(z)}{\mu m_H (1+z)} \right]^3. \quad (14)$$

3.5 Random magnetic field models

We study primordial magnetic fields in the form of randomly oriented cells considering two possible scenarios for the seed field.

Dipole like fields The first scenario we discuss is one where each cell contains a dipole field whose flux is conserved. In this case we have $p = 3/2$ (Hindmarsh & Everett 1998; de Souza & Opher 2008; de Souza & Opher 2010b) in equations (12) and (13).

Ring-like fields We also consider the geometry studied by Ahonen & Enqvist (1998) and Enqvist & Olesen (1993), who found cells with large ring-like fields, but with planes of inclination randomly oriented. Thus, an average over large volumes corresponds to a random walk of all possible inclinations. This is equivalent a random walk on a 2D surface of a sphere, which implies $p = 1$.

3.6 Temperature

In order to calculate the Jeans and filtering masses from equations (4) and (13), it is necessary to have an expression for the evolution of the temperature of the gas with redshift. We use the analytic fit of the temperature as a function of redshift that Kravtsov et al. (2004) obtained for the results of Gnedin (2000),

$$T(z) = \begin{cases} (10^4 \text{ K}) \left(\frac{1+z_s}{1+z} \right)^\alpha, & z > z_s \\ 10^4 \text{ K} & z_s \geq z \geq z_r \\ (10^4 \text{ K}) \left(\frac{1+z}{1+z_r} \right), & z < z_r \end{cases} \quad (15)$$

where $z > z_s$ is the epoch before the first HII regions form, $z_r \leq z \leq z_s$ is the epoch of the overlap of multiple HII regions and $z < z_r$ is the epoch of complete reionization.

Throughout this paper we use $\alpha = 6$, $z_s = 11$ and $z_r = 8$, unless otherwise mentioned.

3.7 Results

We use equations (13), (14) and (15) in (4) to calculate the effect of RPFM on the filtering mass. The results obtained by assuming different values for L_0 and B_0 are shown in figures 1 and 2, for dipole-like fields, and in figures 5 and 6 for ring-like fields (without taking into account the effects of amplification, i.e. setting $f_T^2(z) \approx 1$).

The model proposed by de Souza & Opher (2008) leads to dipole-like field with a comoving $B_0 \approx 0.1 \mu\text{G}$ and $L_0 \approx 1 \text{ pc}$. This curve deviates only slightly from the case

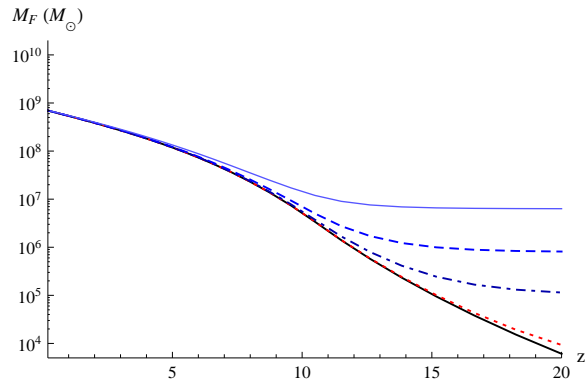


Figure 1. Variation of the filtering mass with redshift in the presence of a dipole-like ($p = 3/2$) random magnetic field, for $z_s = 11$ and $z_r = 8$. The continuous (black) curve corresponds to the $B_0 = 0$ case. The other curves have $B_0 = 0.1 \mu\text{G}$ and, from bottom to top, $L_0 = 10 \text{ pc}$ for the dotted (red) curve; $L_0 = 10^{2.5} \text{ pc}$ for the dash-dotted (dark-blue) curve; $L_0 = 10^{2.5} \text{ pc}$ for the dashed (blue) curve; $L_0 = 10^3 \text{ pc}$ for the thin (light-blue) curve.

of no magnetic field, in figure 1. We found that most models where magnetic fields are generated during a quark-hadron phase transition – which would have dipole-like fields with $B_0 \approx 2 \times 10^{-17} \text{ G}$ and $L_0 \approx 1 \text{ A.U.}$ (Hogan 1983), or $B_0 \approx 10^{-16} \text{ G}$ and $L_0 \approx 1 \text{ pc}$ (Cheng & Olinto 1994) – or during an electroweak phase transition – ring-like fields with $B_0 \sim 10^{-7}$ to 10^{-9} G and $L_0 \sim 10 \text{ A.U.}$ (Baym et al. 1996) – have negligible effects on the filtering mass.

Observations of the cosmic microwave background radiation (CMB) lead to an upper limit on the homogeneous primordial magnetic field $B_{\text{CMB}} = 2.98 \text{ nG}$ (comoving) (Yamazaki et al. 2010) with $L_0 \sim 1 \text{ Mpc}$. This limit corresponds to the brown curve plotted in figures 2, 4, 6 and 8. There is, thus, a family of possible models to explain the origin of cosmic magnetic fields in the early Universe that can create a difference in the filtering mass between $10^4 - 10^{9.5} M_\odot$ and is in agreement with the CMB constraints.

The increase of the filtering mass due to the presence of magnetic fields is bigger before the reionization era, since the temperature, then, contributes less to the total pressure.

We also considered that the seed field could have been amplified by effects of intergalactic turbulence (as discussed in section 3.3). The evolution of the filtering mass considering this effect is shown in figures 3 and 4 for dipole-like fields and 7 and 8 for ring-like fields. Comparing these figures with the previous ones, we note that the amplification leads to an increase in the filtering mass only at small redshifts.

4 GAS FRACTION CONTENT

From numerical simulations, Gnedin (2000) showed that the filtering mass determines the mass fraction of baryonic matter which can be found inside halos. Quantitatively, he found that the fraction, f_g , of the mass of the halo of total mass M , in the form of baryonic gas, can be approximated by the

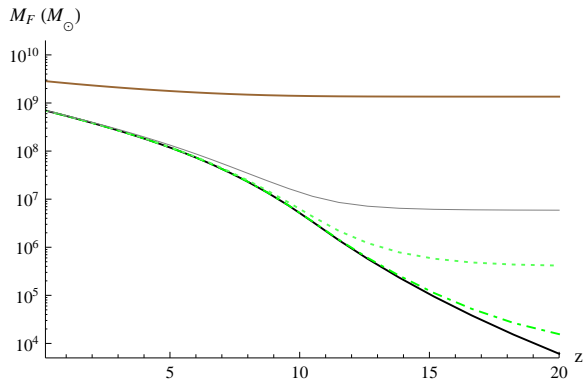


Figure 2. Variation of the filtering mass with redshift in the presence of a dipole-like ($p = 3/2$) random magnetic field, for $z_s = 11$ and $z_r = 8$. The bottom continuous (black) curve corresponds to the $B_0 = 0$ case. The top continuous (brown) curve corresponds to the CMB upper-limit $B_0 \approx 2.98$ nG and $L_0 = 1$ Mpc. The other curves have $B_0 = 10$ nG and, from bottom to top, $L_0 = 10^2$ pc for the dash-dotted (green) curve; $L_0 = 10^3$ pc for the dotted (light-green) curve; $L_0 = 10^4$ pc for the thin (gray) curve.

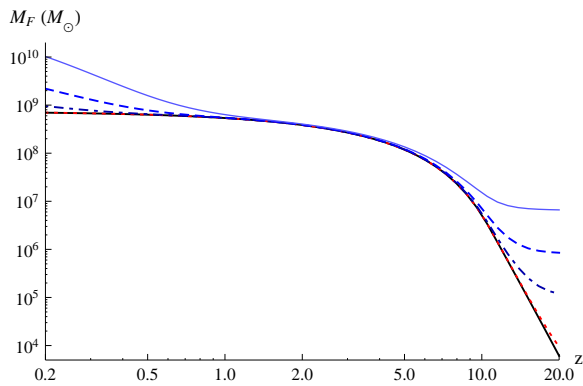


Figure 3. Variation of the filtering mass with redshift in the presence of a dipole-like ($p = 3/2$) random magnetic field, taking into account amplification of the seed fields by IGM turbulence, for $z_s = 11$ and $z_r = 8$. The continuous (black) curve corresponds to the $B_0 = 0$ case. The other curves have $B_0 = 0.1$ μ G and, from bottom to top, $L_0 = 10$ pc for the dotted (red) curve; $L_0 = 10^2$ pc for the dash-dotted (dark-blue) curve; $L_0 = 10^{2.5}$ pc for the dashed (blue) curve; $L_0 = 10^3$ pc for the thin (light-blue) curve.

expression

$$f_g \approx \frac{f_b}{[1 + 0.26M_F(t)/M]^3} \quad (16)$$

where $f_b = \frac{\Omega_b}{\Omega_m}$ is the cosmic baryon to mass fraction.

Using our expression for the magnetic Jeans mass, we evaluate the gas fraction for different values of B_0 and L_0 . We also considered two possible geometries for the seed field and the possibility of the seed field to be amplified by IGM turbulence. The results are presented in figures 9, 10.

As expected, we find a dramatic decrease in the gas fraction for small mass halos, due to the presence of the magnetic field. The fraction of gas can be changed by 2-3 orders of magnitude at high redshift depending on the value of B_0 and the coherence length of the primordial magnetic field, L_0 .

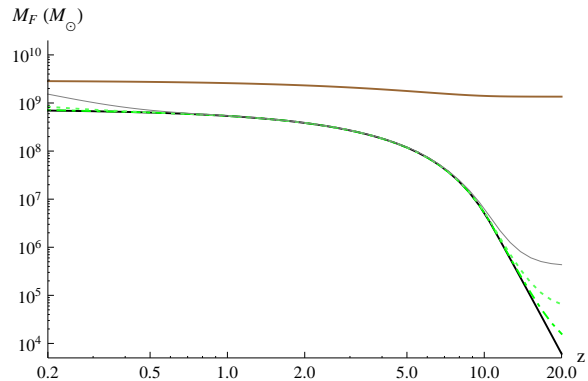


Figure 4. Variation of the filtering mass with redshift in the presence of a dipole-like ($p = 3/2$) random magnetic field, taking into account amplification of the seed fields by IGM turbulence, for $z_s = 11$ and $z_r = 8$. The bottom continuous (black) curve corresponds to the $B_0 = 0$ case. The top continuous (brown) curve corresponds to the CMB upper-limit $B_0 \approx 2.98$ nG and $L_0 = 1$ Mpc. The other curves have $B_0 = 10$ nG and, from bottom to top, $L_0 = 10^2$ pc for the dash-dotted (green) curve; $L_0 = 10^{2.5}$ pc for the dotted (light-green) curve; $L_0 = 10^3$ pc for the thin (gray) curve.

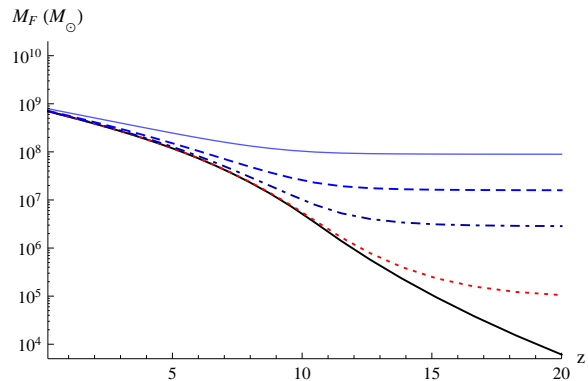


Figure 5. Variation of the filtering mass with redshift in the presence of a ring-like ($p = 1$) random magnetic field, for $z_s = 11$ and $z_r = 8$. The continuous (black) curve corresponds to the $B_0 = 0$ case. The other curves have $B_0 = 0.1$ μ G and, from bottom to top, $L_0 = 10$ pc for the dotted (red) curve; $L_0 = 10^2$ pc for the dash-dotted (dark-blue) curve; $L_0 = 10^{2.5}$ pc for the dashed (blue) curve; $L_0 = 10^3$ pc for the thin (light-blue) curve.

5 CONCLUSIONS

We modified the Jeans mass in order to take into account the presence of random primordial magnetic fields (RPMF) in the form of randomly oriented cells with dipole and ring-like structures. From this modified Jeans mass, we obtained the filtering mass and the baryonic gas fraction of a dark matter halo. We showed that, depending on the magnetogenesis model, which determines B_0 and L_0 , both the Jeans mass and the baryonic gas fraction can change by orders of magnitude. We found, for example, for a comoving $B_0 = 0.1$ μ G, and a reionization epoch that starts at $z_s = 11$ and ends at $z_e = 8$, for $L_0 = 100$ pc at $z = 12$, the f_g becomes severely depressed for $M < 10^7 M_\odot$, whereas for $B_0 = 0$ the f_g becomes severely depressed only for much smaller masses, $M < 10^5 M_\odot$.

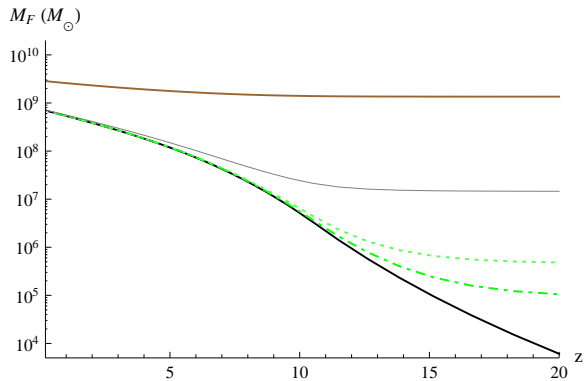


Figure 6. Variation of the filtering mass with redshift in the presence of a ring-like ($p = 1$) random magnetic field, for $z_s = 11$ and $z_r = 8$. The bottom continuous (black) curve corresponds to the $B_0 = 0$ case. The top continuous (brown) curve corresponds to the CMB upper-limit $B_0 \approx 2.98$ nG and $L_0 = 1$ Mpc. The other curves have $B_0 = 10$ nG and, from bottom to top, $L_0 = 10^2$ pc for the dash-dotted (green) curve; $L_0 = 10^3$ pc for the dotted (light-green) curve; $L_0 = 10^4$ pc for the thin (gray) curve.

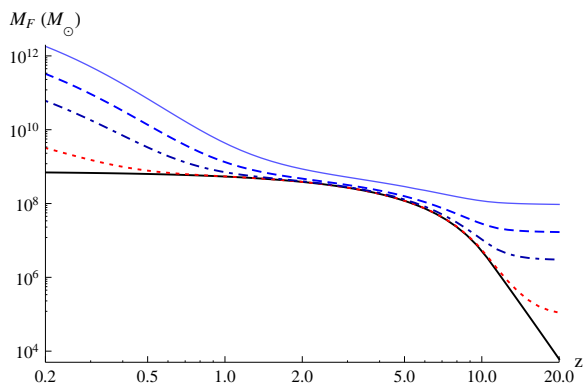


Figure 7. Variation of the filtering mass with redshift in the presence of a ring-like ($p = 1$) random magnetic field, taking into account amplification of the seed fields by IGM turbulence, for $z_s = 11$ and $z_r = 8$. The continuous (black) curve corresponds to the $B_0 = 0$ case. The other curves have $B_0 = 0.1 \mu\text{G}$ and, from bottom to top, $L_0 = 10$ pc for the dotted (red) curve; $L_0 = 10^2$ pc for the dash-dotted (dark-blue) curve; $L_0 = 10^{2.5}$ pc for the dashed (blue) curve; $L_0 = 10^3$ pc for the thin (light-blue) curve.

Since it is very difficult to make observations of intergalactic magnetic fields at high redshifts, and the constraints imposed by CMB measurements are not very restrictive, we suggest the possibility to add new constraints on a family of models for the primordial magnetic field, by following the redshift evolution of the filtering mass of galaxies.

We also calculated the modified baryonic gas fraction that can also be used as an indirect observable to help us to understand the origin and structure of cosmic magnetic fields.

ACKNOWLEDGMENTS

R.S.S. thanks the Brazilian agency FAPESP for financial support (2009/06770-2). L.F.S.R. thanks the Brazilian

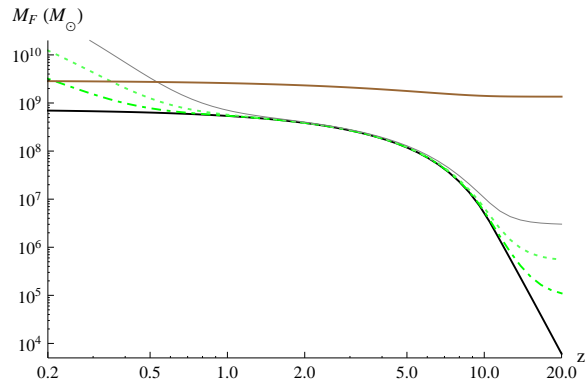


Figure 8. Variation of the filtering mass with redshift in the presence of a ring-like ($p = 1$) random magnetic field, taking into account amplification of the seed fields by IGM turbulence, for $z_s = 11$ and $z_r = 8$. The bottom continuous (black) curve corresponds to the $B_0 = 0$ case. The top continuous (brown) curve corresponds to the CMB upper-limit $B_0 \approx 2.98$ nG and $L_0 = 1$ Mpc. The other curves have $B_0 = 1$ nG and, from bottom to top, $L_0 = 10^2$ pc for the dash-dotted (green) curve; $L_0 = 10^3$ pc for the dotted (light-green) curve; $L_0 = 10^4$ pc for the thin (gray) curve.

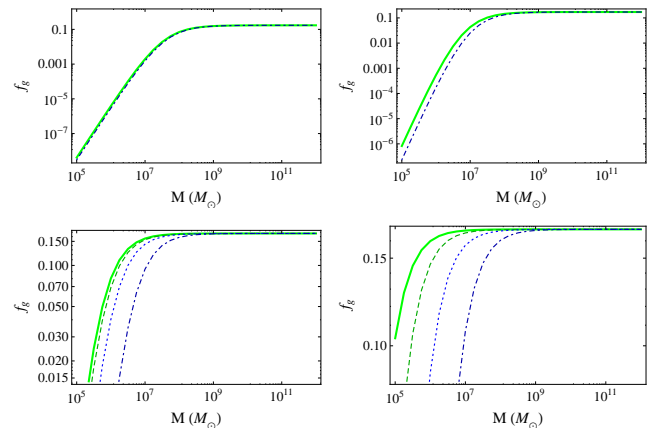


Figure 9. Halo gas fraction, in the presence of a dipole-like field ($p = 3/2$), as a function of halo mass at $z = 3$, $z = 6$, $z = 9$ and $z = 12$, in the top-left, top-right, bottom-left and bottom-right panels, respectively. The thick (green) curve corresponds to $B_0 = 0$. For all other curves, $B_0 = 10^{-7}$ G. For the dashed (dark-green) curve we have $L_0 = 10$ pc, for the dotted (blue) curve, $L_0 = 10^2$ pc, for the dash-dotted (dark-blue) curve, $L_0 = 10^3$ pc.

agency CNPq for financial support (142394/2006-8). R.O. thanks the Brazilian agencies FAPESP (06/56213-9) and CNPq (300414/82-0) for partial support. We also thank all comments of the anonymous referee that helped us to improve the present work.

REFERENCES

- Ahonen J., Enqvist K., 1998, Phys. Rev. D, 57, 664
- Barkana R., Loeb A., 2001, Physics Reports, 349, 125
- Barkana R., Loeb A., 2002, ApJ, 578, 1
- Baym G., Bödeker D., McLerran L., 1996, Phys. Rev. D, 53, 662

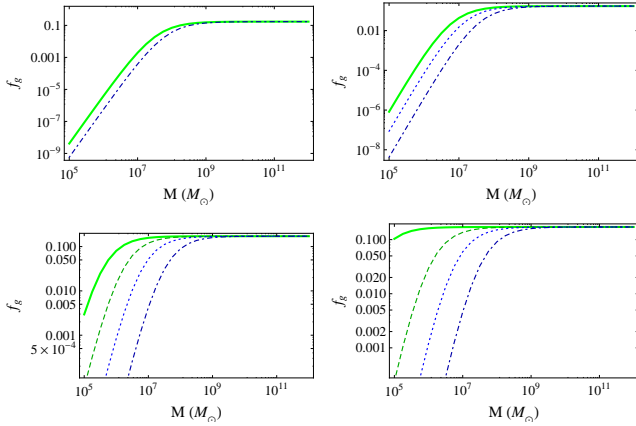


Figure 10. Halo gas fraction, in the presence of a ring-like field ($p = 1$), as a function of halo mass at $z = 3$, $z = 6$, $z = 9$ and $z = 12$, in the *top-left*, *top-right*, *bottom-left* and *bottom-right* panels, respectively. The thick (green) curve corresponds to $B_0 = 0$. For all other curves, $B_0 = 10^{-7}$ G. For the dashed (dark-green) curve we have $L_0 = 10$ pc, for the dotted (blue) curve, $L_0 = 10^2$ pc, for the dash-dotted (dark-blue) curve, $L_0 = 10^3$ pc.

Biermann L., 1950, *Zeitschrift Naturforschung Teil A*, 5
 Cen R., 2003, *ApJ*, 591, L5
 Cheng B., Olinto A. V., 1994, *Phys. Rev. D*, 50, 2421
 Clarke T. E., Kronberg P. P., Boehringer H., 2001, *ApJ*, 547, L111
 Davies G., Widrow L. M., 2000, *The Astrophysical Journal*, 540, 755
 de Souza R., Opher R., 2008, *Physical Review D*, 77, 043528
 de Souza R. S., Opher R., 2010a, *Journal of Cosmology and Astro-Particle Physics*, 2, 22
 de Souza R. S., Opher R., 2010b, *Physical Review D*, 81, 067301
 Enqvist K., Olesen P., 1993, *Physics Letters B*, 319, 178
 Furlanetto S. R., Oh S. P., 2006, *ApJ*, 652, 849
 Gnedin N. Y., 2000, *ApJ*, 542, 535
 Gnedin N. Y., Hui L., 1998, *MNRAS*, 296, 44
 Grasso D., Rubinstein H., 2001, *Physics Reports*, 348, 163
 Haiman Z., Holder G. P., 2003, *ApJ*, 595, 1
 Han J. L., 2008, *Nuclear Physics B - Proceedings Supplements*, 175, 62
 Hanayama H., Takahashi K., Kotake K., Oguri M., Ichiki K., Ohno H., 2005, *ApJ*, 633, 941
 Hindmarsh M., Everett A., 1998, *Physical Review D*, 58, 103505
 Hogan C. J., 1983, *Physical Review Letters*, 51, 1488
 Ichiki K., Takahashi K., Ohno H., Hanayama H., Sugiyama N., 2006, *Sci.*, 311, 827
 Iliev I. T., Scannapieco E., Martel H., Shapiro P. R., 2003, *MNRAS*, 341, 81
 Iliev I. T., Scannapieco E., Shapiro P. R., 2005, *ApJ*, 624, 491
 Kravtsov A. V., Gnedin O. Y., Klypin A. A., 2004, *ApJ*, 609, 482
 Kronberg P. P., 1994, *Reports on Progress in Physics*, 57, 325
 Kuhlen M., Madau P., Montgomery R., 2006, *ApJ*, 637, L1
 Kulsrud R. M., Zweibel E. G., 2008, *Reports on Progress*

in *Physics*, 71, 046901
 Laganá T. F., de Souza R. S., Keller G. R., 2010, *A&A*, 510, A76
 Macciò A. V., Kang X., Fontanot F., Somerville R. S., Koposov S., Monaco P., 2010, *MNRAS*, 402, 1995
 McQuinn M., Lidz A., Zahn O., Dutta S., Hernquist L., Zaldarriaga M., 2007, *MNRAS*, 377, 1043
 Maeda S., Kitagawa S., Kobayashi T., Shiromizu T., 2009, *Classical and Quantum Gravity*, 26, 135014
 Miranda O., Opher M., Opher R., 1998, *MNRAS*, 301, 547
 Naoz S., Barkana R., 2008, *MNRAS*, 385, L63
 Naoz S., Noter S., Barkana R., 2006, *MNRAS*, 373, L98
 Padmanabhan T., 2002, *Theoretical Astrophysics: Volume III: Galaxies and Cosmology*. Cambridge University Press
 Peebles P. J. E., 1967, *ApJ*, 147, 859
 Rees M. J., Reinhardt M., 1972, *A&A*, 19
 Rodrigues L. F. S., de Souza R. S., Opher R., 2010, *MNRAS*, 406, 482
 Ryu D., Kang H., Cho J., Das S., 2008, *Science*, 320, 909
 Schleicher D. R. G., Banerjee R., Klessen R. S., 2008, *Phys. Rev. D*, 78, 083005
 Shapiro P. R., Ahn K., Alvarez M. A., Iliev I. T., Martel H., Ryu D., 2006, *ApJ*, 646, 681
 Takahashi K., Ichiki K., Ohno H., Hanayama H., 2005, *Physical Review Letters*, 95, 4
 Takahashi K., Ichiki K., Ohno H., Hanayama H., Sugiyama N., 2006, *Astronomische Nachrichten*, 327, 410
 Tashiro H., Sugiyama N., 2005, *MNRAS*, 368, 965
 Wasserman I., 1978, *ApJ*, 224, 337
 Widrow L. M., 2002, *Reviews of Modern Physics*, 74, 775
 Wytke J. S. B., Loeb A., 2003, *ApJ*, 588, L69
 Yamazaki D. G., Ichiki K., Kajino T., Mathews G. J., 2010, *Phys. Rev. D*, 81, 023008
 Zweibel E. G., Heiles C., 1997, *Nat.*, 385, 131

This paper has been typeset from a \TeX / \LaTeX file prepared by the author.